Pressure effects on the Fermi surface of Ti-doped CsV_3Sb_5

Kyryl Shtefiienko,[1,*] Cole Phillips,[1,*] Matthew J. Stitz,[2] Ganesh Pokharel,[2,3] Stephen D. Wilson,[3] David E. Graf,[4,5] and Keshav Shrestha[1,†]

[1]*Department of Chemistry and Physics, West Texas A&M University, Canyon, Texas 79016, USA*
[2]*Perry College of Mathematics, Computing, and Sciences, University of West Georgia, Carrollton, Georgia 30118, USA*
[3]*Materials Department, University of California, Santa Barbara, Santa Barbara, California 93106, USA*
[4]*National High Magnetic Field Laboratory, Tallahassee, Florida 32310, USA*
[5]*Department of Physics, Florida State University, Tallahassee, Florida 32306, USA*

(Received 17 March 2025; revised 14 May 2025; accepted 5 June 2025; published 20 June 2025)

This work investigates the Fermi surface of the Ti-doped CsV_3Sb_5 superconductor under pressures up to 2.1 GPa. Upon the application of both chemical and physical pressure in $CsTi_{0.1}V_{2.9}Sb_5$, the superconducting transition temperature increases to $T_c = 6.5$ K, nearly three times higher than that of the parent compound. To probe the Fermi surface under pressure, *in situ* magnetoresistance (MR) measurements are performed in magnetic fields up to 18 T at four pressure points: 0.25, 0.47, 1.55, and 2.1 GPa. The MR data at 0.25 GPa reveal clear Shubnikov–de Haas oscillations with frequency components at $F_\alpha = 21$ T, $F_\beta = 83$ T, $F_\gamma = 709$ T, and $F_\delta = 804$ T. These quantum oscillation frequencies, which correspond to extremal cross-sectional areas of the Fermi surface, vanish above 0.47 GPa, strongly indicating a pressure-induced Fermi surface reconstruction. To interpret these results, we conduct density functional theory calculations of the electronic band structure and Fermi surface. The calculations show a shift in Dirac points and Van Hove singularities near the Fermi level, along with notable changes in the Fermi surface topology as Ti doping increases, confirming that Ti substitution effectively tunes the electronic structure of CsV_3Sb_5. Our combined experimental and theoretical study offers valuable insight into how both chemical and physical pressure can be used to engineer the electronic structure of $CsTi_{0.1}V_{2.9}Sb_5$, providing a pathway for tuning correlated phenomena in kagome superconductors.

DOI: 10.1103/5brw-yxvt

I. INTRODUCTION

Recently, kagome materials with corner-sharing kagome lattices have become the focus of research as they offer promising platforms for exploring emergent quantum phenomena, including superconductivity, charge density wave (CDW) order, nontrivial topology, and geometrically frustrated magnetism [1–4]. Several families of kagome compounds have been discovered [5–10]. One notable family is the AV_3Sb_5 family (A = K, Rb, and Cs), where vanadium atoms form a corner-sharing hexagonal lattice. The materials in this family exhibit superconductivity with critical temperatures ranging from $T_c = 0.3$ to 3 K, alongside a CDW order that emerges below $T_{CDW} \sim 80 - 110$ K [11,12]. The electronic band structure of AV_3Sb_5 features flat bands, multiple Dirac points, and Van Hove singularities near the Fermi level [13–16]. The nontrivial topological nature of AV_3Sb_5 has been revealed through Berry phase analysis and topologically invariant calculations [17–20]. Because of the nontrivial topology along with the presence of superconductivity, AV_3Sb_5 could be an ideal platform for the search of Majorana fermions. The presence of a zero-bias conductance peak in the tunneling experiment of CsV_3Sb_5 supports the idea for topological superconductivity and hence Majorana fermions [21].

Pressure, both chemical and physical, is a powerful tool for tuning the physical properties of materials [22,23]. This approach has been widely used to induce or suppress the tuning of various electronic phases. With the application of pressure, the electronic interactions within the material change, ultimately tuning its properties. For instance, in cuprate superconductors, electron or hole doping induces superconductivity, while in Fe-based superconductors, pressure suppresses the spin density wave state, giving rise to superconductivity [24–29]. The pressure effect in AV_3Sb_5 has recently attracted interest due to its unconventional behavior. Under increasing pressure, the superconducting transition temperature T_c exhibits a nonmonotonic M-shaped dependence on pressure, with two critical pressures at $P_{c1} = 0.7$ GPa and $P_{c2} = 2$ GPa [30–32].

Chemical pressure, achieved by substituting smaller titanium for vanadium sites [33,34], offers an alternative route for tuning the electronic structures of CsV_3Sb_5. It has been found that the CDW phase is suppressed, and T_c also exhibits the double-dome feature. Several studies have already explored chemical doping and high-pressure techniques in CsV_3Sb_5 to tune its CDW and superconducting phases. Various elements, such as titanium, tin, sulfur, chromium, and molybdenum, have been used to substitute either vanadium or antimony sites in the lattice, effectively modifying these

*These authors contributed equally to this work.
†Contact author: kshrestha@wtamu.edu

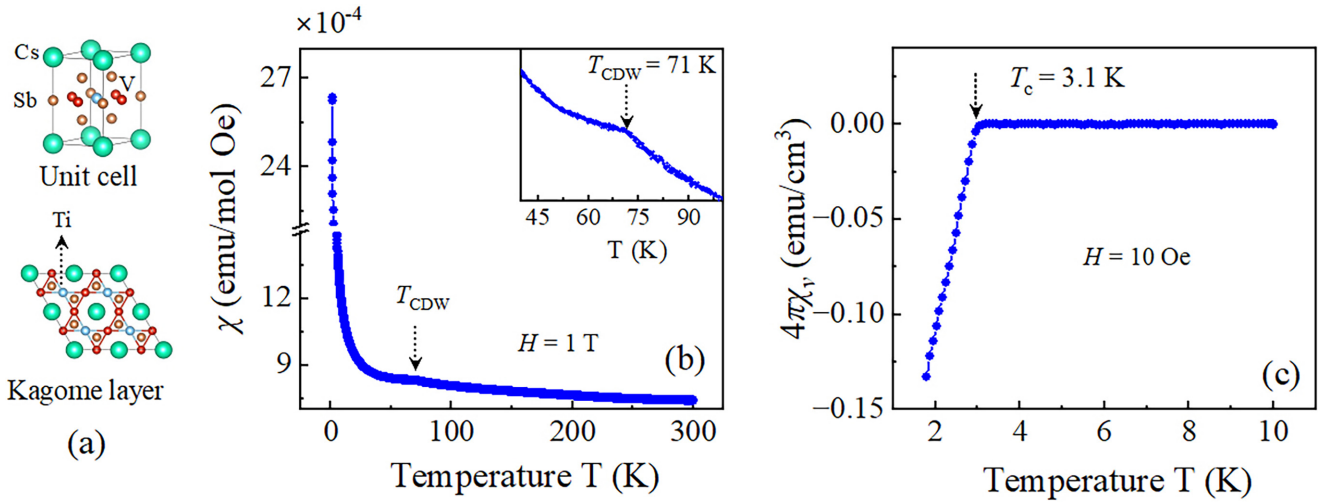

FIG. 1. (a) Unit cell (top) and kagome layer (bottom) of the Ti-doped CsV_3Sb_5 compound. (b) Temperature dependence of magnetic susceptibility $\chi(T)$ for $CsTi_{0.1}V_{2.9}Sb_5$ measured under a magnetic field of $H = 1$ T. The inset shows a close-up of the $\chi(T)$ data. A tiny anomaly near 71 K is observed, indicating a charge density wave. (c) The $\chi(T)$ at low temperatures below 10 K with $H = 10$ Oe, showing superconductivity with an onset critical temperature of $T_c = 3.1$ K.

quantum states [35–39]. In some cases, high pressure has been employed alongside chemical doping to further influence the phase behavior. For instance, Hou *et al.* [34] investigated the temperature-pressure T-P phase diagram of Ti-doped CsV_3Sb_5 under high pressure. However, how the Fermi surface evolves under pressure in these doped systems remains unexplored.

In this work, we focus on the electronic structure of Ti-doped CsV_3Sb_5 by measuring Shubnikov–de Haas (SdH) oscillations under varying pressures. Magnetoresistance (MR) measurements performed in fields up to 18 T reveal clear SdH oscillations with four distinct frequency components. Notably, these frequencies vanish when pressure exceeds 0.47 GPa. According to Onsager's relation [40,41], the frequencies of quantum oscillations are directly related to the extremal cross-sectional areas of the Fermi surface. Thus, the disappearance of these frequencies at higher pressures suggests a significant reconstruction of the electronic structure and Fermi surface in Ti-doped CsV_3Sb_5. Our density functional theory (DFT) calculations qualitatively support these experimental findings.

II. METHODOLOGY

Single crystals of Ti-doped CsV_3Sb_5 were grown via a conventional flux-based growth technique. The details of the sample growth are provided in the Supplemental Material (SM) [42]. The platelike single crystals were gently separated from the flux in an open atmosphere and subsequently cleaned with ethanol. The crystals remained relatively stable in air for short periods of exposure. The phase purity and Ti-doping level were examined using scanning electron microscopy and x-ray-diffraction measurements. Energy-dispersive spectroscopy analysis confirmed the stoichiometry of Cs:Ti:V:Sb as 1:0.1:2.9:5.

Magnetic susceptibility χ measurements on the Ti-doped CsV_3Sb_5 single crystal were conducted using a Quantum Design Magnetic Property Measurement System over the temperature range of 1.8 – 300 K. High-field measurements with maximum fields of 18 T and temperatures as low as 0.3 K were carried out at the SCM-2 facility of the National High Magnetic Field Laboratory in Tallahassee, Florida. A shiny regular-shaped piece of Ti-doped CsV_3Sb_5 single crystal was selected, and four electrical contacts were applied for standard resistivity measurements. The sample was carefully mounted inside a piston-cylinder pressure cell for high-pressure experiments. Daphne 7474 oil was used as the pressure-transmitting medium, and the pressure inside the cell at low temperatures was calibrated by measuring the fluorescence of a small ruby chip placed inside the cell. A fiber-optic cable was embedded with the electrical wires to enable ruby fluorescence measurements inside the pressure cell. The sample was oriented such that the magnetic field was parallel to the c axis of the crystal. Magnetic fields up to 18 T were applied while the sample was under pressure, and the field was swept at each fixed temperature at a rate of 0.3 T/min.

The electronic structure and Fermi surface of Ti-doped CsV_3Sb_5 were computed using WIEN2K [43], based on the full-potential linearized augmented plane wave method within the DFT framework. The generalized gradient approximation with the Perdew-Burke-Ernzerhof parametrization [44] was employed to treat all electrons. The energy convergence criterion was set to 10^{-4} Ry for the self-consistent calculation. The atomic sphere radius (reduced muffin-tin radius) was 2.50 bohrs for Cs, V, Ti, and Sb. Fermi surfaces were generated using a dense **k**-point mesh of $25 \times 25 \times 12$.

III. RESULTS AND DISCUSSION

Figure 1(b) shows the temperature dependence of the magnetic susceptibility $\chi(T)$ for $CsTi_{0.1}V_{2.9}Sb_5$. As seen in the graph, $\chi(T)$ exhibits a paramagneticlike behavior, consistent with that of the parent compound CsV_3Sb_5 [12]. A minor humplike feature appears near 70 K, which is attributed to the charge density wave order. This feature is more clearly visible in the zoomed-in $\chi(T)$ data shown in the inset, where a distinct anomaly is observed near $T_{CDW} = 71$ K due to the

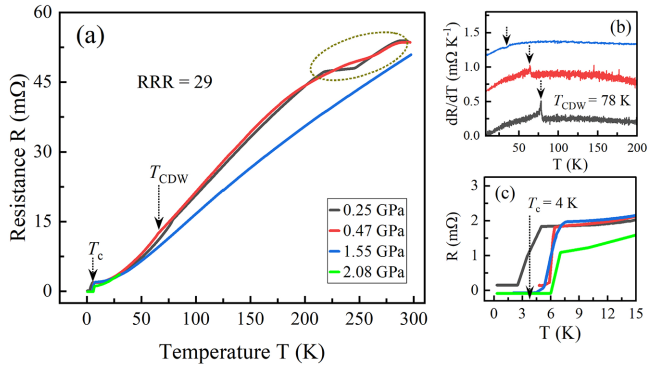

FIG. 2. (a) Temperature dependence of electrical resistance $R(T)$ for $CsTi_{0.1}V_{2.9}Sb_5$ at different external pressures. The $R(T)$ decreases with temperature and exhibits anomalies around 80 and 5 K, as indicated by the dashed arrows, corresponding to CDW and superconducting transitions, respectively. The anomaly near 250 K, indicated by the dotted area, is extrinsic and results from a fast cooling effect. (b) First derivative curves of $R(T)$ at different pressures, emphasizing the CDW transition. (c) Superconducting critical temperature T_c as a function of pressure, showing an increase in T_c with higher pressure.

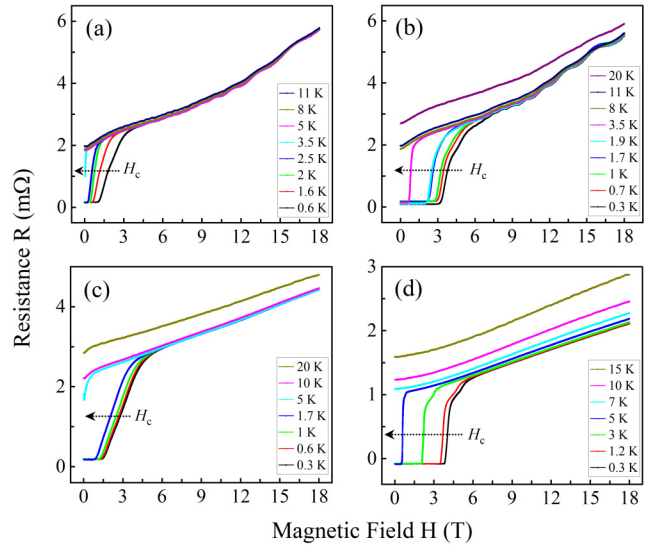

FIG. 3. Magnetoresistance curves at selected temperatures for the Ti-doped CsV_3Sb_5 sample under different pressures: (a) 0.25 GPa, (b) 0.47 GPa, (c) 1.55 GPa, and (d) 2.1 GPa. The MR data reveal a critical field H_c marking the transition from the superconducting to the normal state. The H_c decreases to the lower-field value at higher temperatures, as indicated by the dashed arrow. At high magnetic fields above 7 T, SdH oscillations are observed; however, these oscillations vanish at higher pressures (1.55 and 2.1 GPa).

CDW transition. This T_{CDW} value is lower than the 94 K observed for the parent compound CsV_3Sb_5, likely due to the chemical pressure effect induced by Ti doping.

Figure 1(c) displays the $\chi(T)$ data below 10 K measured under an applied field of $H = 10$ Oe. The diamagnetic signal associated with superconductivity emerges at $T_c^{onset} = 3.1$ K. The superconducting volume fraction reaches approximately 14% diamagnetic at 1.8 K. Our systematic doping study reveals that a bulk superconducting state with nearly 100% shielding fraction is achieved for a slightly higher Ti-doping level, $CsTi_{0.15}V_{2.85}Sb_5$, which will be reported elsewhere. The T_c value of 3.1 K is higher than the 2.5 K reported for the parent compound CsV_3Sb_5 [45]. The increase in T_c along with the suppression of the CDW phase clearly indicates that titanium substitutes vanadium atoms in the crystal lattice, acting as a source of chemical pressure. To further tune the electronic properties of this material, we applied physical pressure using a piston-cylinder pressure clamp.

Figure 2(a) displays the temperature dependence of electrical resistance R for the Ti-doped CsV_3Sb_5 sample under different applied pressures. The resistance decreases with temperature, indicating metallic behavior. The residual resistivity ratio is 29, confirming the high quality of the single crystals used here. A subtle change in slope near 80 K marks the CDW-like transition, while a sharp drop in resistance below 10 K signals the superconducting transition. The CDW-like transition is more pronounced in the derivative data, shown in Fig. 2(b). The transition temperature T_{CDW} is 78 K at 0.25 GPa and shifts to lower temperatures with increasing pressure, becoming barely visible at 1.55 GPa. This gradual suppression of the CDW phase is consistent with previous observations in the parent compound CsV_3Sb_5 and related kagome materials KV_3Sb_5 and RbV_3Sb_5 [46–48].

Interestingly, although a CDW generally opens a gap on part of the Fermi surface and may reduce the carrier density, the resistivity of $CsTi_{0.1}V_{2.9}Sb_5$ decreases more rapidly below the CDW transition [Fig. 2(b)]. This behavior is consistent with the parent compound CsV_3Sb_5 [12,49] where the formation of the CDW leads to a suppression of electron-phonon scattering, resulting in enhanced carrier mobility that offsets the partial loss of carriers. Similar effects have also been reported in the classical CDW system $TiSe_2$ [50].

Figure 2(c) shows the $R(T)$ curves at low temperatures, illustrating the evolution of T_c with pressure. At 0.25 GPa, the onset T_c is 4 K, as indicated by the dashed arrow. The T_c increases to higher values with increasing pressure, reaching a maximum of 6.5 K at 2.1 GPa, which is twice as high as at ambient pressure [Fig. 1(a)] and nearly three times higher than that of the parent compound. Notably, we do not observe the nonmonotonic M-shaped pressure dependence of T_c reported in the parent compound [30,31]. To observe this feature in $CsTi_{0.1}V_{2.9}Sb_5$, we might need a systematic study with finely spaced pressure increments.

To investigate the effect of the magnetic field on the superconducting state of $CsTi_{0.1}V_{2.9}Sb_5$, we applied external magnetic fields up to 18 T *in situ* under pressure. Figure 3 presents the magnetic field dependence of electrical resistance at four different pressures: 0.25, 0.47, 1.55, and 2.1 GPa. At 0.25 GPa, the resistance remains zero at low magnetic fields in the superconducting state but increases sharply above 3 T, indicating a transition to the normal state [Fig. 3(a)]. The critical field H_c for this transition is approximately 2 T at 0.5 K and it gradually decreases at higher temperatures, as indicated by the dashed arrow. At 3.5 K, $H_c = 0.07$ T and superconductivity disappears above this temperature. Furthermore, H_c increases with increasing pressure. For example, $H_c \sim 2$ T at 0.25 GPa and increases to around 5 T at 2.1 GPa. We also note that the transition from the superconducting to the normal state

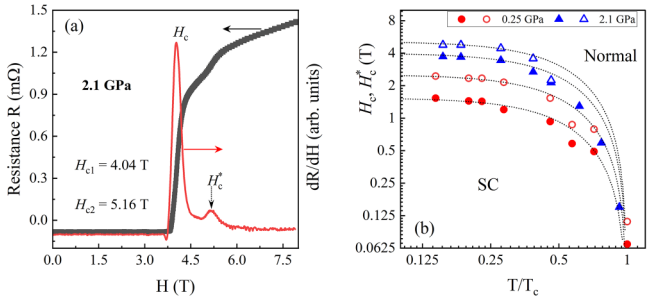

FIG. 4. (a) Resistance R versus magnetic field H data in the low-field region at 2.1 GPa for the $CsTi_{0.1}V_{2.9}Sb_5$ compound. The left y axis shows the raw $R(H)$ data and the right y axis the first derivative of $R(H)$. Two distinct peaks appear at $H_c = 4.04$ T and $H_c^* = 5.16$ T, corresponding to two kinks in the raw data. (b) Temperature dependence of H_c and H_c^* at 0.25 GPa and 2.1 GPa, showing an increase in the critical field at higher pressure. The dashed curves are the fitting curves obtained by using the empirical GL equation. The x and y axes are in logarithmic scale for better visibility.

is broader at lower pressures and becomes sharper at higher pressures, as exemplified at 2.1 GPa [Fig. 3(d)]. Moreover, there appear to be two critical fields for the superconducting-to-normal state transition. This feature has also been observed [51] in the parent compound CsV_3Sb_5.

As mentioned earlier regarding Fig. 3, there is a signature of two critical fields in the superconducting-to-normal state transition. To investigate this further, we analyze the first derivative of the $R(H)$ curve in the low-field region. For example, we present both the raw data and the first derivative curve at 2.1 GPa in Fig. 4(a). Two clear peaks appear near $H_c = 4.04$ T and $H_c^* = 5.16$ T, confirming the presence of two critical fields. The temperature dependence of H_c and H_c^* is shown in Fig. 4(b). For better visibility, we present data only at two pressure points: 0.25 and 2.1 GPa. As seen in the figure, both critical fields gradually decrease with increasing temperature. The temperature dependence of the critical fields at other pressure points is presented in Fig. S2 of the SM [42] and follows similar trends.

Two critical-field-like features have also been observed in the parent compound CsV_3Sb_5 in both in-plane and out-of-plane directions [51]. One possible explanation is the coexistence of two superconducting phases, CsV_3Sb_5 and Ti-doped CsV_3Sb_5 within the sample, each exhibiting different critical fields. The similar temperature dependence of H_c and H_c^* supports this possibility. However, a detailed theoretical study would be beneficial in further understanding this behavior.

The temperature dependence of the critical fields can be described by the empirical Ginzburg-Landau (GL) equation $H_c(T) = H_c(0)(1-t^2)/(1+t^2)$, where $H_c(T)$, $H_c(0)$, and t represent the critical field at temperature T, the critical field at 0 K, and the reduced temperature T/T_c, respectively. The dashed curves in Fig. 4(b) are the best-fit curves to the data using the GL equation. From these best-fit curves, we have estimated the values of the critical field $H_c(0)$ and tabulated them in Table I. As shown in the table, both $H_c(0)$ and $H_c^*(0)$ initially increase from 0.25 GPa to 0.47 GPa, then decrease from 0.47 GPa to 1.55 GPa, and finally increase again

TABLE I. Critical fields at zero temperature.

Pressure (GPa)	$H_c(0)$ (T)	$H_c^*(0)$ (T)
0.25	1.54	2.53
0.47	3.53	4.85
1.55	2.01	3.35
2.1	4.0	5.13

with further pressure increase. This behavior of the critical field is consistent with previous high-pressure studies of the parent compound CsV_3Sb_5 [30,31]. The addition of data at more pressure points could help form a clearer picture of the pressure dependence of these critical fields.

Using the pressure dependent data (Fig. 3), we finally constructed the pressure-temperature T-P phase diagram as presented in Fig. 5. For superconducting transition, all three temperature points, the zero point, midpoint, and onset point, represented as T_c^{zero}, T_c^{mid}, and T_c^{onset}, respectively, are shown in the graph. As seen in the graph, the CDW phase is gradually suppressed at higher pressure and disappears above 1.55 GPa. In the meantime, the superconducting phase becomes more stable at higher pressure. The critical temperature $T_c = 3.1$ K at ambient pressure and it increases nearly by double, to 6.5 K at 2.1 GPa. The T_c shows a monotonic increase with pressure up to 2.1 GPa, which is the maximum pressure range for this experiment. The T_c-P phase diagram shows a double-dome-like feature [30,31] for the parent compound CsV_3Sb_5. We expect that $CsTi_{0.1}V_{2.9}Sb_5$ may exhibit similar behavior; however, our current data lack sufficient pressure points,

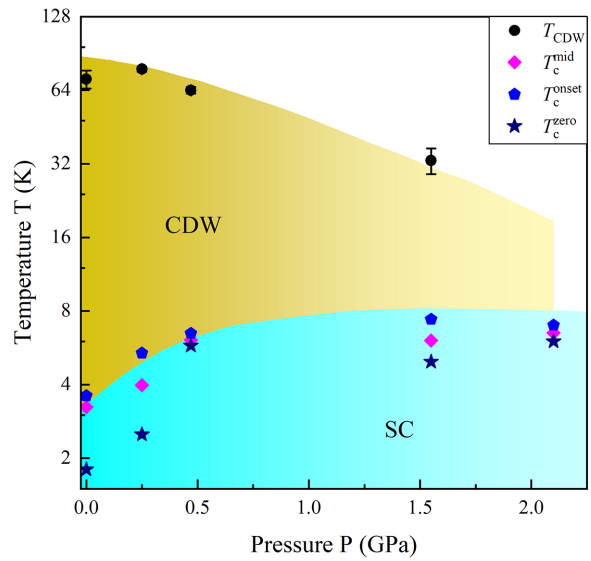

FIG. 5. Temperature-pressure T-P phase diagram of $CsTi_{0.1}V_{2.9}Sb_5$. The zero point, midpoint, and onset point of the critical temperature are represented as T_c^{zero}, T_c^{mid}, and T_c^{onset}, respectively. The charge density wave transition temperature T_{CDW} gradually decreases with pressure and disappears after 1.55 GPa, while the superconducting transition temperature increases gradually at higher pressures. The T_c and T_{CDW} data at ambient pressure are obtained from the magnetic measurements (Fig. 1). The error bar for T_{CDW} is taken as half the width of the transition.

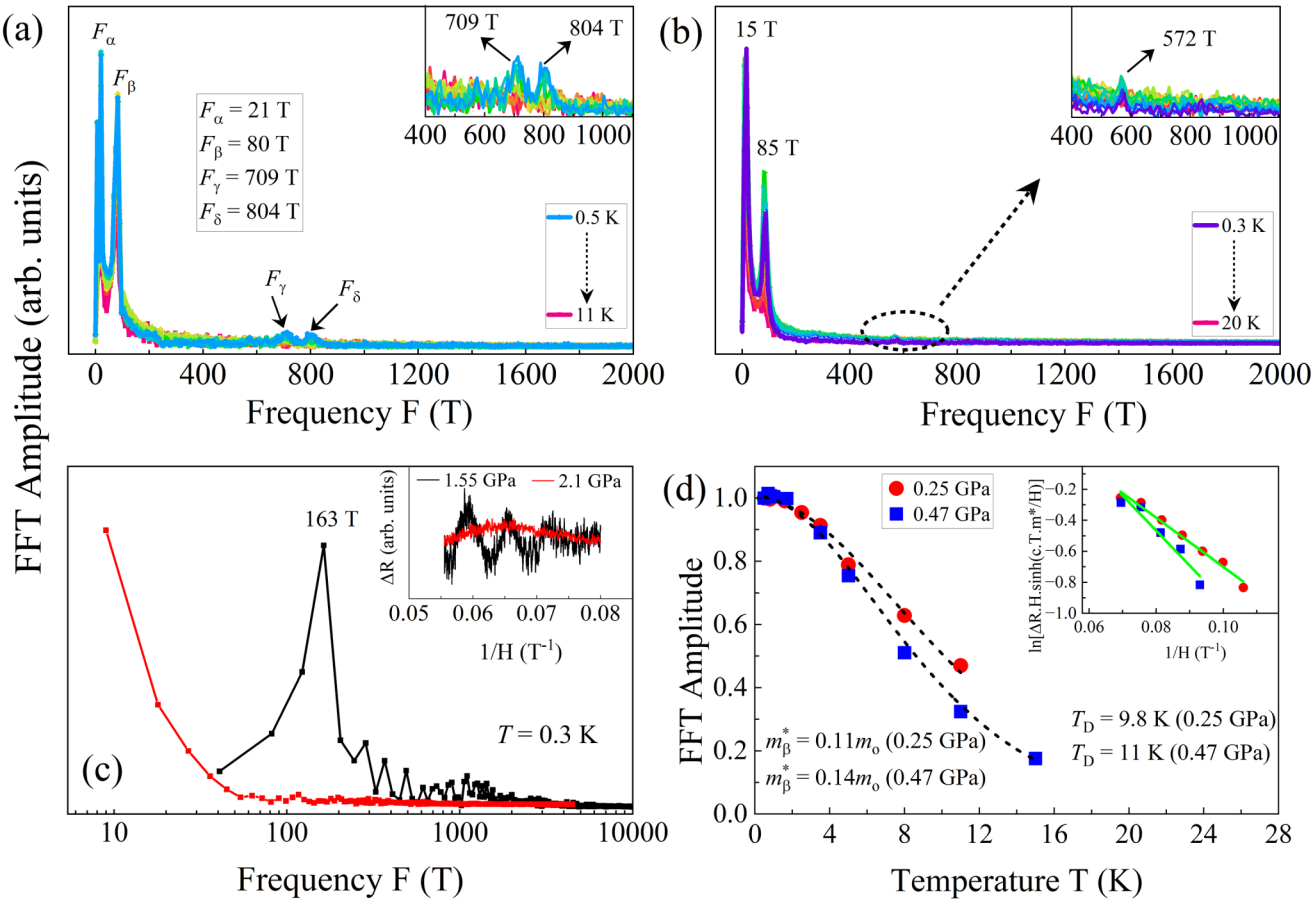

FIG. 6. Frequency spectrum of $CsTi_{0.1}V_{2.9}Sb_5$ at pressures of (a) 0.25 GPa and (b) 0.47 GPa. At 0.25 GPa, four prominent peaks are observed at $F_\alpha = 21$ T, $F_\beta = 83$ T, $F_\gamma = 709$ T, and $F_\delta = 804$ T. The insets in (a) and (b) show close-ups of the frequency spectra highlighting high-frequency peaks. (c) Frequency data at 1.55 and 2.1 GPa for SdH oscillations measured at $T = 0.3$ K, as shown in the inset. The tiny SdH oscillation signal is visible at 1.55 GPa, but it is completely absent at 2.1 GPa. (d) Lifshitz-Kosevich analysis of the F_β frequency at 0.25 and 0.47 GPa. The inset shows the Dingle temperature analysis for the β orbit at 0.25 and 0.47 GPa. The scattered points represent the quantum oscillation amplitudes at various magnetic fields, while the solid lines correspond to the best fits using the LK formula (1).

particularly between 0.47 and 1.55 GPa. Future high-pressure studies with finer pressure increments may help reveal the double-dome superconducting feature in this compound.

In many iron-based (pnictide) and cuprate superconductors, T_c typically follows a domelike feature [27,29,52]. Therefore, it is worthwhile to investigate further how T_c changes with pressure above 2.1 GPa. It is important to note that high-pressure studies on Ti-doped CsV_3Sb_5 have also been reported in Ref. [34], where the evolution of the CDW order and superconducting transition temperature T_c under pressure was systematically investigated. Our results on $CsTi_{0.1}V_{2.9}Sb_5$ are consistent with their findings, particularly in the overall pressure-temperature phase diagram and the suppression of the CDW phase with increasing pressure.

As seen in Fig. 3, the magnetoresistance shows clear SdH oscillations at magnetic fields above 5 T. The oscillations are prominent at low temperatures and gradually disappear at higher temperatures. Furthermore, the oscillations are clearly visible at low pressures (0.25 and 0.47 GPa); however, they seem to be absent at higher pressure points (1.55 and 2.1 GPa). To investigate this, we carried out frequency analyses of the magnetoresistance data. For this, we first subtracted a smooth polynomial background and then performed the fast Fourier transform of the background-subtracted data. The process of background subtraction is presented in Fig. S1 of the SM [42].

The frequency spectrum for $CsTi_{0.1}V_{2.9}Sb_5$ at different pressure points is presented in Fig. 6. At 0.25 GPa, there are three clear major peaks at $F_\alpha = 21$ T, $F_\beta = 83$ T, $F_\gamma = 709$ T, and $F_\delta = 804$ T. The high-frequency signals F_γ and F_δ are more clearly visible in the zoomed-in spectrum, as shown in the inset of Fig. 6(a). A more well-defined signal near 728 and 789 T was also observed in the parent compound CsV_3Sb_5 in our recent torque and tunnel diode oscillation studies [13,32] when applied fields were up to 45 T. Therefore, F_γ and F_δ in Fig. 6(a) should be intrinsic. An increase in the magnetic field range above 18 T is necessary to better resolve these high-frequency peaks.

As the pressure increases to 0.47 GPa, F_α decreases to 15 T, while F_β increases to 85 T [Fig. 6(b)]. The high-frequency signal F_γ decreases to 572 T, whereas F_δ remains unresolved [inset in Fig. 6(b)]. With a further increase in pressure beyond 0.47 GPa, F_α, F_β, F_γ, and F_δ vanish, as shown in Fig. 6(c). A weak frequency signal near 163 T appears at 1.55 GPa but becomes unresolvable at 2.1 GPa. According to Onsager's

relation [53,54], the frequency F of quantum oscillations is directly proportional to the cross-sectional area A_F of the Fermi surface as $F = (\hbar/2\pi e)A_F^2$, where $\hbar$ is the reduced Planck constant and e is the charge of an electron. Therefore, the quantum oscillation frequency is a direct measure of the Fermi surface of the material under study. The absence of a high-frequency signal above 0.47 GPa in this study strongly suggests that the material might have undergone a reconstruction above this pressure. The high-pressure study in our recent work [32] on the parent compound also showed this behavior, and we attributed it to Fermi surface reconstruction.

With the increase of temperature, the amplitude of SdH oscillation decreases, which can be explained by the Lifshitz-Kosevich (LK) theory [53,54]. According to the LK theory, the temperature and magnetic field dependences of SdH oscillations are given by

$$\Delta R(T,H) \propto e^{-\lambda_D} \frac{\lambda(T/H)}{\sinh[\lambda(T/H)]}, \tag{1}$$

with $\lambda_D(H) = \frac{2\pi^2 k_B}{\hbar e} m^* \frac{T_D}{H}$ and $\lambda(T/H) = \frac{2\pi^2 k_B}{\hbar e} m^* \frac{T}{H}$. Here T_D, k_B, and m^* represent the Dingle temperature, Boltzmann constant, and effective mass of the charge carriers, respectively. The first term in the formula is the Dingle factor, which describes the attenuation of the oscillations with decreasing field H. The second term explains the weakening of the oscillations at higher temperatures.

The temperature dependence of the frequency amplitude for the β orbit at 0.25 and 0.47 GPa is presented in Fig. 6(d). As shown in the figure, the LK formula fits the frequency vs temperature data very well. From the best-fit curve, we estimate the effective mass of the charge carriers to be $(0.11 \pm 0.02)m_0$ and $(0.14 \pm 0.02)m_0$ at 0.25 and 0.47 GPa, respectively, where m_0 is the rest mass of the electron. These effective mass values are comparable to those reported for AV_3Sb_5 and other kagome systems [10,14,55–61].

The Dingle temperature T_D provides important insights into the scattering rate and can offer information about the nature of the Fermi surface reconstruction observed in this study. Therefore, we have extracted T_D for the β orbit, as presented in the inset of Fig. 6(d). For this, we fit the field dependence of quantum oscillation amplitude using the LK formula in Eq. (1). We find $T_D = 9.8 \pm 0.6$ K at 0.25 GPa and 11 ± 1.6 K at 0.47 GPa. Within our experimental resolution, T_D remains relatively pressure independent. No clear anomaly is observed near the pressure at which the Fermi surface reconstruction occurs, suggesting that the transition is not accompanied by a significant change in quasiparticle scattering.

In order to better understand the experimental observations, we have carried out electronic structure calculations of Ti-doped CsV_3Sb_5 using DFT, as presented in Fig. 7. With the replacement of the vanadium atom by a titanium atom, there is a significant change in the electronic bands, as shown in Figs. 7(a) and 7(b). The parent compound shows a rich number of Dirac points and Van Hove singularities near the Fermi level. These observations are in agreement with previous reports [59,62,63]. The electronic band structure evolves with increasing Ti concentration, leading to noticeable shifts in the Dirac points and Van Hove singularities, as indicated by the arrows and dotted circles.

The Ti-doping effect also changes the Fermi surface, as presented in Fig. 7(c). The Fermi surface of CsV_3Sb_5 consists of a cylinderlike feature at the Γ point, along with chainlike features at the corners of the Brillouin zone. With higher Ti doping, the central cylinderlike feature undergoes a drastic transformation, splitting at the center and shrinking. Similarly, the Fermi surface feature at the corner evolve into cylinderlike shapes, which become larger. Our recent DFT studies under pressure [63] on the parent compound CsV_3Sb_5 revealed a similar evolution of the electronic bands and Fermi surface features under increasing pressure. Therefore, these studies suggest that titanium substitution in CsV_3Sb_5 effectively acts as a source of chemical pressure, tuning the electronic properties of the material in a manner analogous to applied physical pressure.

IV. SUMMARY

We have presented the electronic structure of Ti-doped CsV_3Sb_5 under high pressure by measuring quantum oscillations. Replacing V atoms with Ti acts as a form of chemical pressure, effectively tuning the charge density wave and superconducting phases. The parent compound exhibits superconductivity at $T_c = 2.5$ K and a CDW transition at $T_{CDW} = 91$ K. With light Ti doping in $CsTi_{0.1}V_{2.9}Sb_5$, the CDW transition is suppressed to 71 K, while T_c increases to 3.1 K. Upon applying external pressure up to 2.1 GPa, the CDW phase is completely suppressed and T_c rises to 6.5 K. By combining pressure- and field-dependent measurements of T_{CDW} and T_c, we have constructed the T-P phase diagram for $CsTi_{0.1}V_{2.9}Sb_5$. These observations are consistent with previous studies of CsV_3Sb_5 [33,34,39,48,64–67]. However, to date, no studies have investigated the Fermi surface evolution under pressure in Ti-doped compounds.

To probe the Fermi surface of $CsTi_{0.1}V_{2.9}Sb_5$, we applied high magnetic fields up to 18 T *in situ* with applied pressure. Magnetoresistance measurements revealed clear Shubnikov–de Haas oscillations, with four dominant frequencies: $F_\alpha = 21$ T, $F_\beta = 83$ T, $F_\gamma = 709$ T, and $F_\delta = 804$ T. As the pressure increased, these frequency peaks vanished above 0.47 GPa. According to Onsager's relation [40,41], quantum oscillation frequencies are directly proportional to the extremal cross-sectional areas of the Fermi surface. Thus, the disappearance of these oscillations above 0.47 GPa provides strong evidence for a reconstruction of the Fermi surface in $CsTi_{0.1}V_{2.9}Sb_5$.

One might question whether the loss of oscillation signals could arise from nonhydrostatic pressure conditions or inhomogeneity in the pressure medium. However, previous studies have shown that the Daphne 7474 oil used as a pressure medium remains hydrostatic up to 3–4 GPa [32,68,69], well above the maximum pressure of 2.1 GPa applied in our measurements. Therefore, it is unlikely that the disappearance of quantum oscillation frequencies is an experimental artifact.

To support our experimental observations, we carried out electronic structure calculations of Ti-doped CsV_3Sb_5 at various Ti-doping levels using density functional theory. Our results show that with increasing Ti content, the Dirac points and Van Hove singularities shift closer to the Fermi level

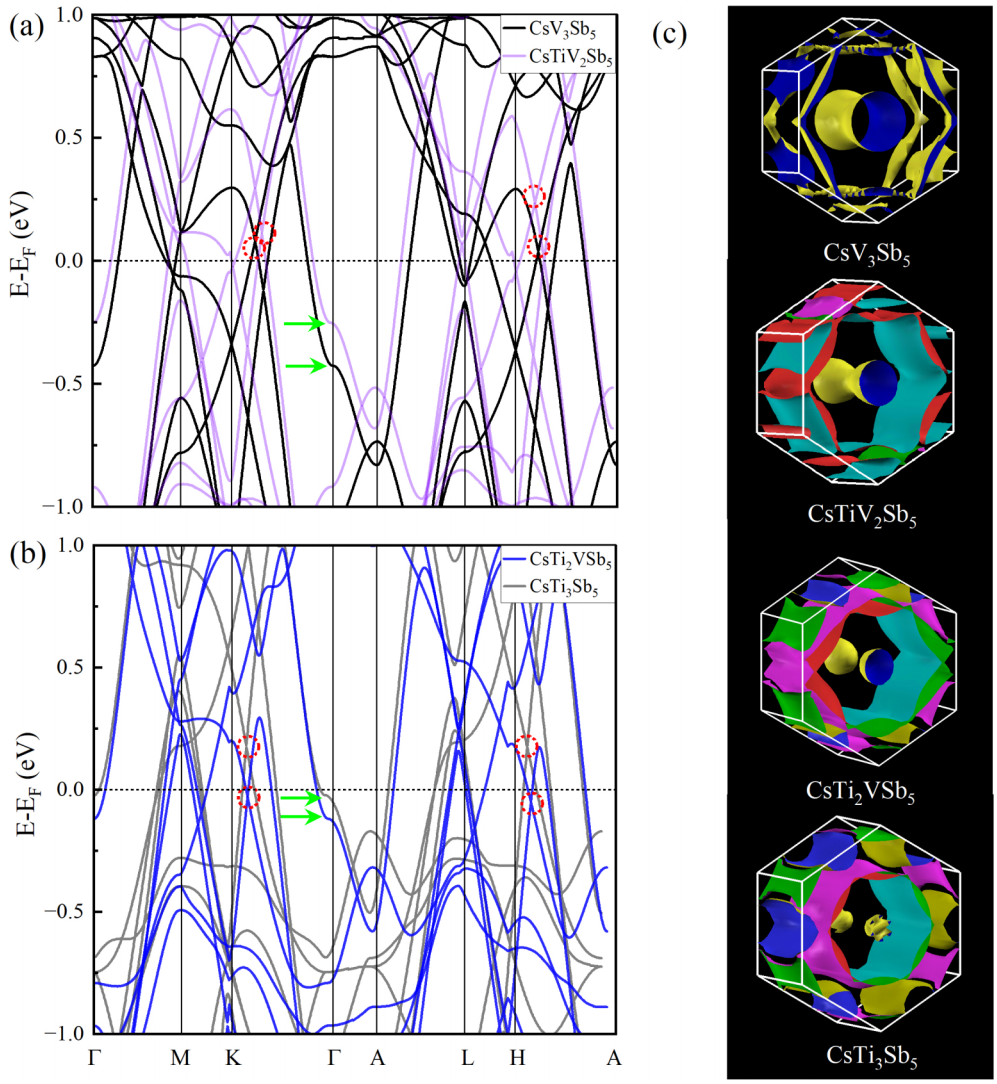

FIG. 7. Electronic band structure of (a) CsV_3Sb_5 and $CsTiV_2Sb_5$ and (b) $CsTi_2VSb_5$ and $CsTi_3Sb_5$. The characteristic electronic features, including the Dirac cone and Van Hove singularity, exhibit a noticeable shift with increasing titanium doping, as indicated by the dashed arrows and dotted circles. (c) Fermi surface of Ti-doped CsV_3Sb_5, showing a clear evolution as the titanium-doping concentration increases. The cylinderlike feature at the center Γ point undergoes a drastic change, splitting at the center and shrinking with higher Ti doping.

and the Fermi surface becomes increasingly distorted. These trends closely mimic the effects typically observed under external pressure [16,63], confirming that Ti doping introduces chemical pressure capable of tuning the electronic structure. Ideally, the origin of the observed SdH frequencies (Fig. 6) could be identified by linking them to specific features of the Fermi surface, as demonstrated in other kagome materials [10,70,71]. However, computing the electronic structure for $CsTi_{0.1}V_{2.9}Sb_5$ at such a low doping level would require constructing a very large supercell, which exceeds our current computational resources.

In summary, the combined experimental and DFT results offer valuable insights into the behavior of CsV_3Sb_5 under both chemical and external pressure. These findings deepen our understanding of kagome compounds and highlight the potential of chemical doping as a tool for engineering electronic structures and quantum states in these materials.

ACKNOWLEDGMENTS

This work was supported in part by the U.S. Department of Energy, Office of Science, Office of Workforce Development for Teachers and Scientists (WDTS) under the Visiting Faculty Program (VFP) at Los Alamos National Laboratory, administered by the Oak Ridge Institute for Science and Education. The work at the West Texas A&M University (WTAMU) is supported by the Killgore Undergraduate and Graduate Student Research Grants, the Welch Foundation (Grant No. AE-0025), and the National Science Foundation (Award ID 2336011). The computations were performed on the WTAMU HPC cluster, which was funded by the National Science Foundation (NSF CC* GROWTH 2018841). G.P. and M.J.S. gratefully acknowledge the support of Dr. James "Earl" Perry CMCS Fund and the University of West Georgia. G. P. and S.D.W. gratefully acknowledge the support via the UC Santa Barbara NSF Quantum Foundry funded via the

Q-AMASE-i program under Award DMR-1906325. A portion of this work was performed at the National High Magnetic Field Laboratory, which is supported by National Science Foundation Cooperative Agreement No. DMR-2128556 and the State of Florida.

V. DATA AVAILABILITY

The data that support the findings of this article are not publicly available. The data are available from the authors upon reasonable request.

[1] J.-X. Yin, B. Lian, and M. Z. Hasan, Topological kagome magnets and superconductors, Nature (London) **612**, 647 (2022).

[2] S. D. Wilson and B. R. Ortiz, AV_3Sb_5 kagome superconductors, Nat. Rev. Mater. **9**, 420 (2024).

[3] Y. Wang, H. Wu, G. T. McCandless, J. Y. Chan, and M. N. Ali, Quantum states and intertwining phases in kagome materials, Nat. Rev. Phys. **5**, 635 (2023).

[4] K. Shtefiienko, C. Phillips, S. Mozaffari, R. P. Madhogaria, W. R. Meier, D. G. Mandrus, D. E. Graf, and K. Shrestha, Electronic structure of YV_6 Sn_6 probed by de Haas–van Alphen oscillations and density functional theory, APL Quantum **2**, 016118 (2025).

[5] K. Shtefiienko, C. Phillips, B. R. Ortiz, D. E. Graf, and K. Shrestha, Electronic structure of the kagome metal $YbTi_3Bi_4$ studied using torque magnetometry, Phys. Rev. B **111**, 035145 (2025).

[6] G. Pokharel, S. M. L. Teicher, B. R. Ortiz, P. M. Sarte, G. Wu, S. Peng, J. He, R. Seshadri, and S. D. Wilson, Electronic properties of the topological kagome metals YV_6Sn_6 and GdV_6Sn_6, Phys. Rev. B **104**, 235139 (2021).

[7] J. Lee and E. Mun, Anisotropic magnetic property of single crystals RV_6Sn_6 (R = Y, Gd–Tm, Lu), Phys. Rev. Mater. **6**, 083401 (2022).

[8] S. Peng, Y. Han, G. Pokharel, J. Shen, Z. Li, M. Hashimoto, D. Lu, B. R. Ortiz, Y. Luo, H. Li *et al.*, Realizing kagome band structure in two-dimensional kagome surface states of RV_6Sn_6 (R = Gd, Ho), Phys. Rev. Lett. **127**, 266401 (2021).

[9] E. Rosenberg, J. M. DeStefano, Y. Guo, J. S. Oh, M. Hashimoto, D. Lu, R. J. Birgeneau, Y. Lee, L. Ke, M. Yi *et al.*, Uniaxial ferromagnetism in the kagome metal TbV_6Sn_6, Phys. Rev. B **106**, 115139 (2022).

[10] K. Shrestha, B. Regmi, G. Pokharel, S.-G. Kim, S. D. Wilson, D. E. Graf, B. A. Magar, C. Phillips, and T. Nguyen, Electronic properties of kagome metal ScV_6Sn_6 using high-field torque magnetometry, Phys. Rev. B **108**, 245119 (2023).

[11] B. R. Ortiz, L. C. Gomes, J. R. Morey, M. Winiarski, M. Bordelon, J. S. Mangum, I. W. H. Oswald, J. A. Rodriguez-Rivera, J. R. Neilson, S. D. Wilson *et al.*, New kagome prototype materials: Discovery of KV_3Sb_5, RbV_3Sb_5, and CsV_3Sb_5, Phys. Rev. Mater. **3**, 094407 (2019).

[12] B. R. Ortiz, S. M. L. Teicher, Y. Hu, J. L. Zuo, P. M. Sarte, E. C. Schueller, A. M. M. Abeykoon, M. J. Krogstad, S. Rosenkranz, R. Osborn *et al.*, CsV_3Sb_5: A $\mathbb{Z}_2$ topological kagome metal with a superconducting ground state, Phys. Rev. Lett. **125**, 247002 (2020).

[13] K. Shrestha, R. Chapai, B. K. Pokharel, D. Miertschin, T. Nguyen, X. Zhou, D. Y. Chung, M. G. Kanatzidis, J. F. Mitchell, U. Welp *et al.*, Nontrivial fermi surface topology of the kagome superconductor CsV_3Sb_5 probed by de Haas–van Alphen oscillations, Phys. Rev. B **105**, 024508 (2022).

[14] K. Shrestha, M. Shi, T. Nguyen, D. Miertschin, K. Fan, L. Deng, D. E. Graf, X. Chen, and C.-W. Chu, Fermi surface mapping of the kagome superconductor RbV_3Sb_5 using de Haas–van Alphen oscillations, Phys. Rev. B **107**, 075120 (2023).

[15] K. Shrestha, M. Shi, B. Regmi, T. Nguyen, D. Miertschin, K. Fan, L. Z. Deng, N. Aryal, S.-G. Kim, D. E. Graf *et al.*, High quantum oscillation frequencies and nontrivial topology in kagome superconductor KV_3Sb_5 probed by torque magnetometry up to 45 T, Phys. Rev. B **107**, 155128 (2023).

[16] S. R. Bhandari, M. Zeeshan, V. Gusain, K. Shrestha, and D. Rai, First-principles study of the electronic structure, Z_2 invariant, and quantum oscillation in the kagome material CsV_3Sb_5, APL Quantum **1**, 046118 (2024).

[17] W. Zhang, L. Wang, C. W. Tsang, X. Liu, J. Xie, W. C. Yu, K. T. Lai, and S. K. Goh, Emergence of large quantum oscillation frequencies in thin flakes of the kagome superconductor CsV_3Sb_5, Phys. Rev. B **106**, 195103 (2022).

[18] D. Chen, B. He, M. Yao, Y. Pan, H. Lin, W. Schnelle, Y. Sun, J. Gooth, L. Taillefer, and C. Felser, Anomalous thermoelectric effects and quantum oscillations in the kagome metal CsV_3Sb_5, Phys. Rev. B **105**, L201109 (2022).

[19] C. Broyles, D. Graf, H. Yang, X. Dong, H. Gao, and S. Ran, Effect of the interlayer ordering on the fermi surface of kagome superconductor CsV_3Sb_5 revealed by quantum oscillations, Phys. Rev. Lett. **129**, 157001 (2022).

[20] Z. Wang, W. Zhang, L. Wang, T. F. Poon, C. W. Tsang, W. Wang, J. Xie, S. T. Lam, X. Zhou, Y. Zhao *et al.*, Similarities and differences in the fermiology of kagome metals AV_3Sb_5 (A= K, Rb, Cs) revealed by Shubnikov–de Haas oscillations, Appl. Phys. Lett. **123**, 012601 (2023).

[21] Z. Liang, X. Hou, F. Zhang, W. Ma, P. Wu, Z. Zhang, F. Yu, J.-J. Ying, K. Jiang, L. Shan *et al.*, Three-dimensional charge density wave and surface-dependent vortex-core states in a kagome superconductor CsV_3Sb_5, Phys. Rev. X **11**, 031026 (2021).

[22] B. Lorenz and C. Chu, in *Frontiers in Superconducting Materials*, edited by A. V. Narlikar (Springer, Berlin, 2005), pp. 459–497.

[23] M. Xu, Y. Li, and Y. Ma, Materials by design at high pressures, Chem. Sci. **13**, 329 (2022).

[24] A. Dewaele and L. Nataf, Magnetic phase diagram of iron at high pressure and temperature, Phys. Rev. B **106**, 014104 (2022).

[25] I. Levatić, P. Popčević, V. Šurija, A. Kruchkov, H. Berger, A. Magrez, J. S. White, H. M. Rønnow, and I. Živković, Dramatic pressure-driven enhancement of bulk skyrmion stability, Sci. Rep. **6**, 21347 (2016).

[26] L. Deng, H.-C. Wu, A. P. Litvinchuk, N. F. Yuan, J.-J. Lee, R. Dahal, H. Berger, H.-D. Yang, and C.-W. Chu, Room-temperature skyrmion phase in bulk Cu_2OSeO_3 under high pressures, Proc. Natl. Acad. Sci. USA **117**, 8783 (2020).

[27] H. Takahashi, A. Sugimoto, Y. Nambu, T. Yamauchi, Y. Hirata, T. Kawakami, M. Avdeev, K. Matsubayashi, F. Du, C. Kawashima *et al.*, Pressure-induced superconductivity in the iron-based ladder material $BaFe_2S_3$, Nat. Mater. **14**, 1008 (2015).

[28] J. Zhang, S. Zhang, H. Weng, W. Zhang, L. Yang, Q. Liu, S. Feng, X. Wang, R. Yu, L. Cao *et al.*, Pressure-induced superconductivity in topological parent compound Bi_2Te_3, Proc. Natl. Acad. Sci. USA **108**, 24 (2011).

[29] K. Shrestha, L. Deng, K. Zhao, B. Jawdat, B. Lv, B. Lorenz, and C. Chu, Doping dependence and high-pressure studies on $Eu_xCa_{1-x}Fe_2As_2$ ($0 \leqslant x \leqslant 1$), Supercond. Sci. Technol. **33**, 095010 (2020).

[30] F. Yu, D. Ma, W. Zhuo, S. Liu, X. Wen, B. Lei, J. Ying, and X. Chen, Unusual competition of superconductivity and charge-density-wave state in a compressed topological kagome metal, Nat. Commun. **12**, 3645 (2021).

[31] K. Y. Chen, N. N. Wang, Q. W. Yin, Y. H. Gu, K. Jiang, Z. J. Tu, C. S. Gong, Y. Uwatoko, J. P. Sun, H. C. Lei *et al.*, Double superconducting dome and triple enhancement of T_c in the kagome superconductor CsV_3Sb_5 under high pressure, Phys. Rev. Lett. **126**, 247001 (2021).

[32] C. Phillips, K. Shtefiienko, T. Nguyen, A. N. Capa Salinas, B. A. Magar, G. Pokharel, S. D. Wilson, D. E. Graf, and K. Shrestha, Fermi surface reconstruction under pressure in the kagome metal CsV_3Sb_5, Phys. Rev. B **110**, 205135 (2024).

[33] H. Yang, Z. Huang, Y. Zhang, Z. Zhao, J. Shi, H. Luo, L. Zhao, G. Qian, H. Tan, B. Hu *et al.*, Titanium doped kagome superconductor $CsV_{3-x}Ti_xSb_5$ and two distinct phases, Sci. Bull. **67**, 2176 (2022).

[34] J. Hou, K. Y. Chen, J. P. Sun, Z. Zhao, Y. H. Zhang, P. F. Shan, N. N. Wang, H. Zhang, K. Zhu, Y. Uwatoko *et al.*, Effect of hydrostatic pressure on the unconventional charge density wave and superconducting properties in two distinct phases of doped kagome superconductors $CsV_{3-x}Ti_xSb_5$, Phys. Rev. B **107**, 144502 (2023).

[35] K. J. Zhu, L. P. Nie, B. Lei, M. J. Wang, K. L. Sun, Y. Z. Deng, M. L. Tian, T. Wu, and X. H. Chen, Competitive superconductivity and charge density wave in Mo-doped kagome superconductor CsV_3Sb_5, Phys. Rev. Res. **6**, 023295 (2024).

[36] S. Yousuf, J. Song, H. Jang, V. T. A. Hong, T. Lee, N. ul Ain, S. YH, Y. Kim, H. Lee, and T. Park, Synthesis and physical properties of Cr-doped kagome superconductor CsV_3Sb_5, Curr. Appl. Phys. **61**, 7 (2024).

[37] F. Song, C. Ke, Y. Liu, T. Weng, C.-C. Hsieh, C. H. Cheng, Y. Chen, and Y. Zhao, Effect of sulfur doping on superconductivity and charge density wave order in kagome metal $CsV_3(Sb_{1-x}S_x)_5$, Supercond. Sci. Technol. **38**, 015010 (2025).

[38] Y. Liu, Y. Wang, Y. Cai, Z. Hao, X.-M. Ma, L. Wang, C. Liu, J. Chen, L. Zhou, J. Wang *et al.*, Doping evolution of superconductivity, charge order, and band topology in hole-doped topological kagome superconductors $Cs(V_{1-x}Ti_x)_3Sb_5$, Phys. Rev. Mater. **7**, 064801 (2023).

[39] Y. M. Oey, B. R. Ortiz, F. Kaboudvand, J. Frassineti, E. Garcia, R. Cong, S. Sanna, V. F. Mitrović, R. Seshadri, and S. D. Wilson, Fermi level tuning and double-dome superconductivity in the kagome metal $CsV_3Sb_{5-x}Sn_x$, Phys. Rev. Mater. **6**, L041801 (2022).

[40] C. Kittel and P. McEuen, *Introduction to Solid State Physics* (Wiley, New York, 2018).

[41] N. W. Ashcroft and N. Mermin, *Solid State Physics* (Holt, Rinehart and Winston, New York, 1976), Vol. 1, Appendix C.

[42] See Supplemental Material at http://link.aps.org/supplemental/10.1103/5brw-yxvt for experimental details, Shubnikov–de Haas oscillations analyses, and the critical magnetic fields for Ti-doped CsV_3Sb_5.

[43] P. Blaha, K. Schwarz, G. K. H. Madsen, D. Kvasnicka, and J. Luitz, *WIEN2k*: *An Augmented Plane Wave Plus Local Orbitals Program for Calculating Crystal Properties* (Vienna University of Technology, Vienna, 2001), p. 60.

[44] J. P. Perdew, K. Burke, and M. Ernzerhof, Generalized gradient approximation made simple, Phys. Rev. Lett. **77**, 3865 (1996).

[45] K. Jiang, T. Wu, J.-X. Yin, Z. Wang, M. Z. Hasan, S. D. Wilson, X. Chen, and J. Hu, Kagome superconductors AV_3Sb_5 (A = K, Rb, Cs), Natl. Sci. Rev. **10**, nwac199 (2023).

[46] F. Du, S. Luo, R. Li, B. R. Ortiz, Y. Chen, S. D. Wilson, Y. Song, and H. Yuan, Evolution of superconductivity and charge order in pressurized RbV_3Sb_5, Chin. Phys. B **31**, 017404 (2022).

[47] C. C. Zhu, X. F. Yang, W. Xia, Q. W. Yin, L. S. Wang, C. C. Zhao, D. Z. Dai, C. P. Tu, B. Q. Song, Z. C. Tao *et al.*, Double-dome superconductivity under pressure in the V-based kagome metals AV_3Sb_5 (A = Rb and K), Phys. Rev. B **105**, 094507 (2022).

[48] X. Chen, X. Zhan, X. Wang, J. Deng, X.-B. Liu, X. Chen, J.-G. Guo, and X. Chen, Highly robust reentrant superconductivity in CsV_3Sb_5 under pressure, Chin. Phys. Lett. **38**, 057402 (2021).

[49] H. Zhao, H. Li, B. R. Ortiz, S. M. Teicher, T. Park, M. Ye, Z. Wang, L. Balents, S. D. Wilson, and I. Zeljkovic, Cascade of correlated electron states in the kagome superconductor CsV_3Sb_5, Nature (London) **599**, 216 (2021).

[50] F. J. Di Salvo, D. Moncton, and J. Waszczak, Electronic properties and superlattice formation in the semimetal $TiSe_2$, Phys. Rev. B **14**, 4321 (1976).

[51] R. Chapai, A. E. Koshelev, M. P. Smylie, D. Y. Chung, A. Kayani, K. Bhatt, G. Rimal, M. G. Kanatzidis, W.-K. Kwok, J. Mitchell, and U. Welp, Origin of the unusual temperature dependence of the upper critical field of kagome superconductor CsV_3Sb_5: Multiple bands or van Hove singularities? arXiv:2411.16625.

[52] X. Zhou, W.-S. Lee, M. Imada, N. Trivedi, P. Phillips, H.-Y. Kee, P. Törmä, and M. Eremets, High-temperature superconductivity, Nat. Rev. Phys. **3**, 462 (2021).

[53] Y. Ando, Topological insulator materials, J. Phys. Soc. Jpn. **82**, 102001 (2013).

[54] D. Shoenberg, *Magnetic Oscillations in Metals* (Cambridge University Press, Cambridge, 2009).

[55] F. H. Yu, T. Wu, Z. Y. Wang, B. Lei, W. Z. Zhuo, J. J. Ying, and X. H. Chen, Concurrence of anomalous Hall effect and charge density wave in a superconducting topological kagome metal, Phys. Rev. B **104**, L041103 (2021).

[56] Q. Yin, Z. Tu, C. Gong, Y. Fu, S. Yan, and H. Lei, Superconductivity and normal-state properties of kagome metal RbV_3Sb_5 single crystals, Chin. Phys. Lett. **38**, 037403 (2021).

[57] S.-Y. Yang, Y. Wang, B. R. Ortiz, D. Liu, J. Gayles, E. Derunova, R. Gonzalez-Hernandez, L. Šmejkal, Y. Chen, S. S. Parkin *et al.*, Giant, unconventional anomalous Hall effect in the metallic frustrated magnet candidate, KV_3Sb_5, Sci. Adv. **6**, eabb6003 (2020).

[58] B. R. Ortiz, S. M. L. Teicher, L. Kautzsch, P. M. Sarte, N. Ratcliff, J. Harter, J. P. C. Ruff, R. Seshadri, and S. D. Wilson, Fermi surface mapping and the nature of charge-density-wave order in the kagome superconductor CsV_3Sb_5, Phys. Rev. X **11**, 041030 (2021).

[59] Y. Fu, N. Zhao, Z. Chen, Q. Yin, Z. Tu, C. Gong, C. Xi, X. Zhu, Y. Sun, K. Liu *et al.*, Quantum transport evidence of topological band structures of kagome superconductor CsV_3Sb_5, Phys. Rev. Lett. **127**, 207002 (2021).

[60] K. Shrestha, V. Marinova, B. Lorenz, and P. C. W. Chu, Shubnikov–de Haas oscillations from topological surface states of metallic $Bi_2Se_{2.1}Te_{0.9}$, Phys. Rev. B **90**, 241111(R) (2014).

[61] K. Shrestha, V. Marinova, D. Graf, B. Lorenz, and C. W. Chu, Quantum oscillations in metallic Sb_2Te_2Se topological insulator, Phys. Rev. B **95**, 075102 (2017).

[62] M. Kang, S. Fang, J.-K. Kim, B. R. Ortiz, S. H. Ryu, J. Kim, J. Yoo, G. Sangiovanni, D. Di Sante, B.-G. Park *et al.*, Twofold van Hove singularity and origin of charge order in topological kagome superconductor CsV_3Sb_5, Nat. Phys. **18**, 301 (2022).

[63] S. R. Bhandari, V. Gusain, M. Zeeshan, D. Rai, and K. Shrestha, Pressure effects on the electronic structure of the kagome metal CsV_3Sb_5, APL Quantum **2**, 016133 (2025).

[64] X. Wen, F. Yu, Z. Gui, Y. Zhang, X. Hou, L. Shan, T. Wu, Z. Xiang, Z. Wang, J. Ying *et al.*, Emergent superconducting fluctuations in compressed kagome superconductor CsV_3Sb_5, Sci. Bull. **68**, 259 (2023).

[65] Z. Zhang, Z. Chen, Y. Zhou, Y. Yuan, S. Wang, J. Wang, H. Yang, C. An, L. Zhang, X. Zhu *et al.*, Pressure-induced reemergence of superconductivity in the topological kagome metal CsV_3Sb_5, Phys. Rev. B **103**, 224513 (2021).

[66] A. N. Capa Salinas, B. R. Ortiz, C. Bales, J. Frassineti, V. F. Mitrović, and S. D. Wilson, Electron-hole asymmetry in the phase diagram of carrier-tuned CsV_3Sb_5, Front. Electron. Mater. **3**, 1257490 (2023).

[67] J. Liu, Q. Li, Y. Li, X. Fan, J. Li, P. Zhu, H. Deng, J.-X. Yin, H. Yang, J. Li *et al.*, Enhancement of superconductivity and phase diagram of Ta-doped kagome superconductor CsV_3Sb_5, Sci. Rep. **14**, 9580 (2024).

[68] N. Tateiwa and Y. Haga, Evaluations of pressure-transmitting media for cryogenic experiments with diamond anvil cell, Rev. Sci. Instrum. **80**, 123901 (2009).

[69] K. Murata, K. Yokogawa, H. Yoshino, S. Klotz, P. Munsch, A. Irizawa, M. Nishiyama, K. Iizuka, T. Nanba, T. Okada *et al.*, Pressure transmitting medium Daphne 7474 solidifying at 3.7 GPa at room temperature, Rev. Sci. Instrum. **79**, 085101 (2008).

[70] D. Miertschin, T. Nguyen, S. R. Bhandari, K. Shtefiienko, C. Phillips, B. A. Magar, R. Sankar, D. E. Graf, and K. Shrestha, Anisotropic quantum transport in ZrSiS probed by high-field torque magnetometry, Phys. Rev. B **110**, 085140 (2024).

[71] Z. Rehfuss, C. Broyles, D. Graf, Y. Li, H. Tan, Z. Zhao, J. Liu, Y. Zhang, X. Dong, H. Yang *et al.*, Quantum oscillations in kagome metals $CsTi_3Bi_5$ and $RbTi_3Bi_5$, Phys. Rev. Mater. **8**, 024003 (2024).